

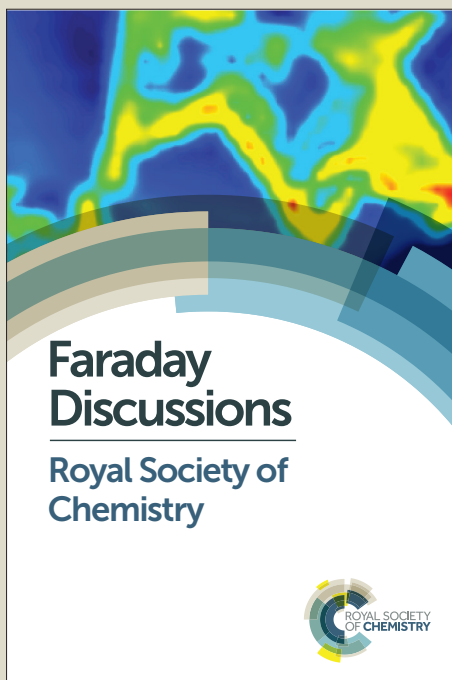
Faraday Discussions

Accepted Manuscript



This manuscript will be presented and discussed at a forthcoming Faraday Discussion meeting. All delegates can contribute to the discussion which will be included in the final volume.

Register now to attend! Full details of all upcoming meetings: <http://rsc.li/fd-upcoming-meetings>



This is an *Accepted Manuscript*, which has been through the Royal Society of Chemistry peer review process and has been accepted for publication.

Accepted Manuscripts are published online shortly after acceptance, before technical editing, formatting and proof reading. Using this free service, authors can make their results available to the community, in citable form, before we publish the edited article. We will replace this *Accepted Manuscript* with the edited and formatted *Advance Article* as soon as it is available.

You can find more information about *Accepted Manuscripts* in the [Information for Authors](#).

Please note that technical editing may introduce minor changes to the text and/or graphics, which may alter content. The journal's standard [Terms & Conditions](#) and the [Ethical guidelines](#) still apply. In no event shall the Royal Society of Chemistry be held responsible for any errors or omissions in this *Accepted Manuscript* or any consequences arising from the use of any information it contains.

Revealing nanocomposites filler structure by swelling and small-angle X-ray scattering

Guilhem P. Baeza^{1,2§}, Anne-Caroline Genix¹, Nathalie Paupy-Peyronnet², Christophe Degrandcourt², Marc Couty^{*2}, and Julian Oberdisse¹

¹ *Laboratoire Charles Coulomb (L2C), UMR 5221 CNRS-Université de Montpellier, F-34095 Montpellier, France*

² *Manufacture Française des Pneumatiques MICHELIN, Site de Ladoux, 23 place des Carmes Déchaux, F-63 040 Clermont-Ferrand, France*

22/7/15

Abstract

Polymer nanocomposites are of widespread use, namely for the industrial application of car tires. The rheological behavior of such nanocomposites depends in a crucial way on the dispersion of the hard filler particles – typically silica nanoparticles embedded in a soft polymer matrix. It is thus important to assess the filler structure, which may be quite difficult for aggregates of nanoparticles of high polydispersity, and with strong interactions at high loading. This has been achieved recently using a coupled TEM/SAXS structural model describing the filler microstructure of simplified industrial nanocomposites with grafted or ungrafted silica of high structural disorder.

Here, we will present an original method capable of reducing inter-aggregate interactions by swelling of nanocomposites, diluting the filler to low volume fractions. Note that this is impossible to reach by solid mixing due to the large differences in viscoelasticity between the composite and the pure polymer. By combining matrix crosslinking, swelling in a good monomer solvent, and post-polymerization of these monomers, it is shown that it is possible to separate the filler into small aggregates. The latter have then been characterized by electron microscopy and small-angle X-ray scattering, confirming the conclusions of the abovementioned TEM-SAXS structural model applied directly to the highly loaded cases.

[§]*Current address: FORTH / IESL - Polymer group, 70013 Heraklion, Crete, Greece*

1. Introduction

Polymer nanocomposites (PNCs) are of widespread use in applications, in particular in the car tire industry.¹ Their mechanical properties are governed by their microstructure and dynamics, which is why model systems where these properties can be easily evidenced are commonly investigated²⁻⁸. In particular the multi-scale microstructure of filler nanoparticles (NPs), which form small aggregates, which themselves can be structured in space and build filler networks, has received considerable attention in the past⁹⁻¹¹. Whatever the experimental approach, direct imaging¹² or scattering techniques¹³, two main difficulties arise: polydispersity in shape and size, and strong interactions. The latter point is obviously related to mechanical reinforcement, which can only be reached if the filler content is high enough. Considerable efforts have therefore been undertaken to unravel the filler structure in PNCs, with quite some success in model systems. On the other hand, less attention was devoted to complex multi-scale filler of industrial origin, and most descriptions remain necessarily limited to a few global quantities like average fractal dimensions¹⁴⁻²⁰.

The standard procedure to synthesize PNCs with high viscosity polymers and precipitated silica is to use solid mixing. The typical size of the filler objects in the composite are commonly supposed to depend on the characteristics of the mixing process like temperature and torque vs. time, and thus on the raw materials used to formulate the composite. In a series of papers²¹⁻²⁴ on filler structure in styrene-butadiene (SB) nanocomposites, we have coupled small-angle X-ray scattering (SAXS) and transmission electron microscopy (TEM) on silica filled PNCs of industrial relevance. A structural model extracting the average aggregation number N_{agg} (the number of primary particle in an aggregate) from combined TEM/SAXS data under the hypothesis of repulsive interactions between aggregates has been proposed²³. Using a fully polydisperse description of aggregate structure and interactions deduced from Monte Carlo simulations, it has been shown that for systems with coating agent and an equal mixture of non-functional and functional polymers, N_{agg} is independent of the silica volume fraction. Conversely, N_{agg} decreases for systems with an increasing amount of functional polymer at constant volume fraction. However, to validate this structural model, the best way would be to reduce interactions – instead of simulating them – in order to access the aggregate structure directly. This could be achieved by diluting the nanocomposite with polymer to low volume fractions. Unfortunately, because of large differences in viscoelasticity between the composite and the pure polymer, solid mixing of both components – polymer and silica – at

low filler volume fraction generates only a dispersion of the original high volume fraction material in the pure polymer matrix.

Swelling nanocomposites with solvents or monomers has been used in the field of intercalating nano-clays²⁵⁻²⁷. Timochenco et al, e.g., show that the interaction peak between clay platelets in X-ray diffraction disappears upon swelling with poly(styrene).²⁵ Boukerrou et al use swelling with aliphatic molecules in order to widen galleries between clay filler for polymerization of epoxy resins and nanocomposite formation.²⁶ Finally, swelling of polymer networks with organic solvents is a commonly used technique used to characterize the entropic elasticity of the network, and thus crosslinking. The latter approach can be extended to the presence of filler nanoparticles and their influence on the network properties.²⁷ Concerning structural studies by small-angle scattering, Shinohara et al have used swelling of SB nanocomposites with industrial filler NPs in organic solvents to conclude qualitatively on the absence of interactions between aggregates.¹⁸ Using imaging techniques with electron microscopy, Sarkawi et al have swollen PNCs based on natural rubber filled with silica in styrene.²⁸ Their objective was two-fold. First, the degree of swelling could be used to analyze the apparent crosslink density. Secondly, the dilution of the filler structure reduced interactions between filler NPs, and thus geometrical overlap, allowing them to conclude on the importance of filler-matrix interaction as a function of coupling agent.

In the present paper, we propose an original experimental approach using SAXS combined with matrix crosslinking of the PNC, swelling in a good polymer 'solvent' – styrene monomers – and post-polymerization of these monomers. We first compare the filler structure of the samples studied here to previously described PNCs in the unswollen state. Then, structure after crosslinking, and after swelling, is investigated using electron microscopy and SAXS, and compared to the results of the structural model applied in presence of interactions.

2. Materials and Methods

Starting materials and nanocomposite preparation. The styrene-butadiene copolymer (with antioxidants 6PPD and AO2246) has been purpose-synthesized by Michelin, and the chain mass characterized by size exclusion chromatography. The polymer matrix is made of two types of chains of molecular mass of ca. $190 \text{ kg}\cdot\text{mol}^{-1}$ and PI below 1.1, see Table 1. Each chain is a statistical copolymer with styrene (27%w) and butadiene (73%w) units (42% of which are 1-2 and 58% of 1-4). One type – termed D3 – carries a single graftable end-function²⁴, whereas the other one (NF) is not functionalized. The glass-transition temperature was measured by differential scanning calorimetry (DSC) (200F3 Maia from Netzsch) with a heating rate of 20 K/min.

Table 1: Characteristics of functionalized and non functionalized polymer molecules.

SB-polymer	D3	NF
T_g (°C)	-36.0	-36.6
M_n (kg mol ⁻¹)	185	174
M_w (kg mol ⁻¹)	197	188
PI	1.07	1.08

Silica-SB nanocomposites have been formulated by stepwise introduction and mixing of SB chains with silica pellets (Zeosil 1165 MP from Solvay, with DPG, Vulcacit from Bayer, and covering agent octeo from Dynasylan) in an internal mixer (Haake) following the same method as before²³. In addition, however, an organic crosslinking agent in very small amount compared to standard crosslinking (dicumyl peroxide, 1 to 5 mg for 8 g of nanocomposite) was added during the external mixing phase (two roll mill) for samples intended for subsequent swelling experiments without dissolving the samples as explained below. Note that any trace of carbon black, catalysing nanoparticles (ZnO), standard vulcanising or coupling agents was avoided, making these simplified industrial nanocomposites suitable for analysis by scattering. After external mixing, samples have been crosslinked by thermal activation in a press at 160°C for 40 minutes. Three series of nanocomposites have been studied. One series at fixed matrix composition of 50%D3 as a function of silica volume fraction Φ_{Si} , and two series in matrix composition, at Φ_{Si} fixed to $\approx 10\%v$ and $\approx 20\%v$, respectively. The real silica volume fractions in the nanocomposites reported here have been measured by thermogravimetric analysis (Mettler Toledo) using a first ramp at 30 K/min from

25°C to 550°C under nitrogen, followed by a second ramp at 20 K/min from 550°C to 750°C under air, and results are given below.

Swelling experiments. Crosslinked nanocomposite disks of thickness 0.6 mm have been immersed for 65 h in styrene monomer mixed with benzoyl peroxide as initiator of styrene polymerisation (polystyrene, PS) after swelling. While the maximum swelling ratio is usually reached after 24h, most homogeneous polymerisation was found by waiting up to 65 h. Polymerisation of the styrene inside the nanocomposites was performed at 100°C during 4 hours. The final samples were flat disks of approximate thickness 1.5 mm. The procedure is shown in Figure 1, together with photographs of the initial nanocomposites and the final samples. Throughout this article, we will refer to final samples as swollen samples (or “after swelling”), meaning that they have undergone the complete crosslinking/swelling/polymerization procedure.

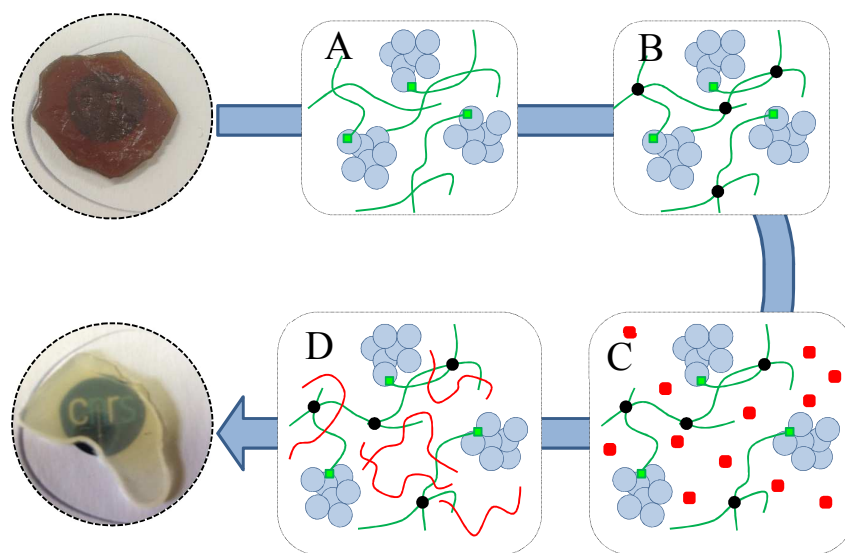


Figure 1: Initial nanocomposites (upper photograph and point A) with schematic representation of the SB-crosslinking (point B; SB in green), the swelling with styrene monomers and initiator (in red, point C) leading to polymerization (point D) where PS is depicted in red. The swollen nanocomposite is shown to be transparent in the lower photograph.

The silica volume fraction in swollen samples has been measured by TGA. The volume swelling ratio for the three nanocomposite series is determined via the silica volume fraction ratio of the initial nanocomposite with respect to the sample with polystyrene, and is reported in Tables 2 and 3. Note that excellent agreement with large- q SAXS normalization (intensity proportional to Φ_{Si}) was found. Concerning the swelling ratios, they are rather scattered

around an average value of ca. 10, without any dominant tendency with silica content and grafting, even if at 16.7%v, higher swelling seems to be obtained for the samples with least grafting.

Table 2: Nanocomposite series in filler volume fraction at fixed matrix composition (50%D3). Φ_{Si} is reported before and after swelling, and the swelling ratio deduced.

Initial Φ_{Si} (%v)	Final Φ_{Si} (%v)	Swelling ratio
8.2	0.8	10.5
13.3	1.8	7.2
16.8	2.0	8.6
21.3	1.1	19.8

Table 3: Nanocomposite series in matrix composition (grafting %D3) at fixed initial silica volume fraction of ca. 8.2%v (left) and 16.7%v (right).

%D3	Initial Φ_{Si} (%v)	Final Φ_{Si} (%v)	Swelling ratio	Initial Φ_{Si} (%v)	Final Φ_{Si} (%v)	Swelling ratio
0	8.3	0.9	9.2	16.8	1.4	11.9
25	8.1	1.1	7.6	16.8	1.6	10.6
50	8.2	0.8	10.5	16.8	2.0	8.6
75	8.1	1.1	7.6	16.7	2.3	7.4
100	8.4	0.7	11.4	16.6	2.3	7.3

Structural characterization. The silica microstructure of the nanocomposites has been studied by electron microscopy and SAXS. TEM pictures were obtained with samples prepared by ultracryomicrotomy at -80°C on a LEICA FC-7 (Diatome ultra 35° , desired thickness set to 50 to 70 nm) with a Philips CM200 LaB6 (200 kV, bright field mode). Scanning electron microscopy (SEM) pictures were obtained with samples prepared using a standard razor blade cut from a macroscopic sample using a SEM Zeiss Ultra 55 (1 kV, secondary electron images with In Lens detector). SAXS experiments (beamline ID02, ESRF, Grenoble) were performed at a wavelength of 1.1 \AA (12.46 keV), using two sample-to-detector distances (1 m and 10 m), yielding a total q-range from 0.001 to 0.5 \AA^{-1} . Even lower-q data was measured on the Bonse-Hart set-up on ID02 ($q_{\min} = 10^{-4} \text{ \AA}^{-1}$). Samples had an approximate thickness of 0.8 mm. The scattering cross section per unit sample volume $d\Sigma/d\Omega$ (in cm^{-1}) – which we term scattered intensity $I(q)$ – was obtained by using standard procedures including background subtraction and calibration given by ESRF. In all cases, both PS-swollen and unswollen matrices have been subtracted. The contrast of silica in SB-polymer for SAXS experiments was calculated from the scattering length densities ($\rho_{SB} =$

$8.85 \cdot 10^{10} \text{ cm}^{-2}$, $\rho_{\text{Si}} = 1.97 \cdot 10^{11} \text{ cm}^{-2}$, $\Delta\rho = 1.09 \cdot 10^{11} \text{ cm}^{-2}$), which were themselves known from the chemical composition. Moreover, contrast between polystyrene with silica ($1.0 \cdot 10^{11} \text{ cm}^{-2}$) is very close to the silica-SB contrast, whereas the styrene-SB contrast is a factor of ten weaker ($0.9 \cdot 10^{10} \text{ cm}^{-2}$). It is thus sufficient to rationalize the data in terms of polymer-silica contrast only, whatever the polymer.

A SAXS form factor analysis of the silica NPs was found to be compatible with a lognormal size distribution ($R_0 = 8.55 \text{ nm}$, $\sigma = 27\%$).²³ The average bead volume is then $V_{\text{Si}} = 3.6 \cdot 10^3 \text{ nm}^3$, which will be used to estimate aggregation numbers of silica NP in aggregates.

3. Results and discussion

The homogeneous distribution of filler nanoparticles throughout the polymer matrix has been checked by SEM in order to qualitatively analyze the material at large length scales. In Figure 2, an example with a matrix composition of 50%D3, and $\Phi_{\text{Si}} = 16.8\%v$ (i.e., native, unswollen PNCs), is shown at low magnification.

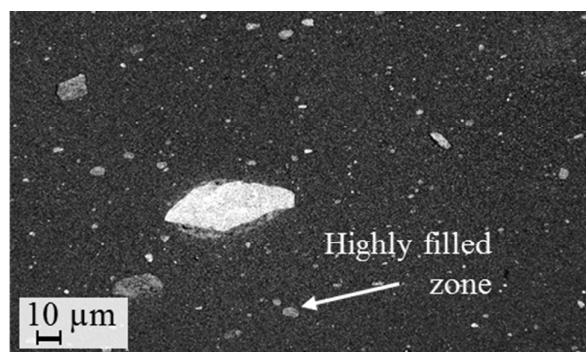


Figure 2: SEM of a silica SB nanocomposite at low magnification showing the presence of highly filled zones ($\Phi_{\text{Si}} = 16.8\%v$, 50%D3).

The majority of the silica NPs is seen to be distributed homogeneously on the scale of microns and tens of microns, as can be seen from the background in Figure 2, which actually has a fine structure of silica distributed homogeneously in the matrix, as well as some highly filled zones. In Figure 3a, a SEM picture of the ‘background’ zones of the same PNC before swelling (cf. Figure 2) is shown at high magnification. A dense assembly of small aggregates of typical radius 50 nm is visible. It is difficult to tell from the 2D picture if they are all

connected, but the filler structure is very similar to the large-scale silica network of aggregates of nanoparticles, or locally connected aggregates with surrounding polymer channels observed by us before^{23, 24}. The micrograph on the right-hand-side, Figure 3b, finally, displays the filler structure of swollen nanocomposites on a local scale. Clearly, the network-type structure is broken up on the scale of aggregates, which appear to be well dispersed in space. If they are somewhat polydisperse in size and shape, it is still surprising that they stay in the same size-range of typically below 100 nm. Thus electron microscopy confirms that the swelling approach separates the filler in homogeneously filled zones. Naturally, swelling is accompanied by a large reduction of the visible silica surface fraction (from Figure 3a to 3b). TGA measurements given in section 2 confirm the dilution of the original ca 17% volume fraction PNCs to around 2%v.

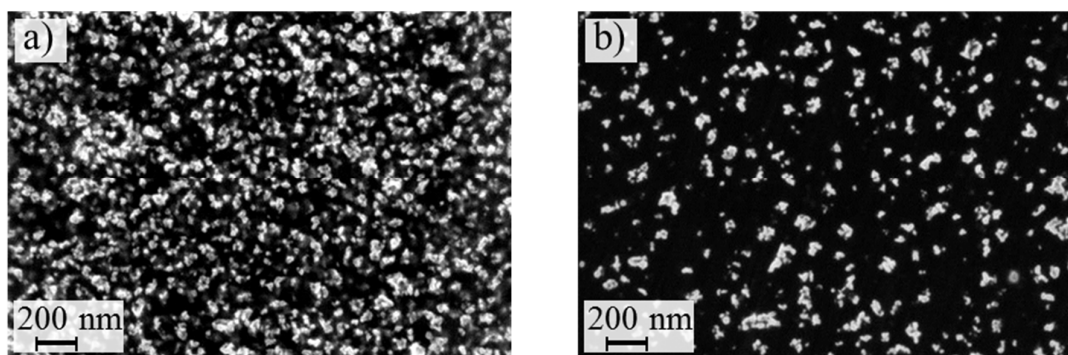


Figure 3: SEM (a) of a silica-SB nanocomposite at high magnification showing the filler network structure ($\Phi_{\text{Si}} = 16.8\%v$, 50%D3), (b) of the same sample after swelling as explained in the text ($\Phi_{\text{Si}} = 2.0\%v$).

In Figure 4, TEM pictures of a swollen sample show more detail on aggregate structure. The completely functionalized nanocomposite is seen to have a typical aggregate size in the sub-100 nm range, corresponding to aggregate radii of 40 or 50 nm on average. One can also count individual silica nanoparticles in order to estimate aggregation numbers, and one finds that there is considerable polydispersity around aggregation numbers of typically several tens. However, it is difficult to conclude on statistically relevant information from these pictures.

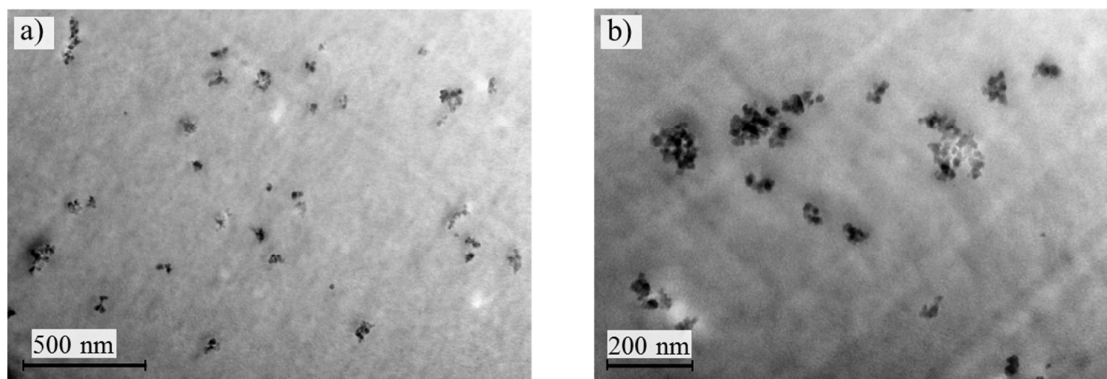


Figure 4: TEM of a functionalized nanocomposite ($\Phi_{\text{Si}} = 16.6\%v$, 100%D3) at different scales (a) 500 nm, and (b) 200 nm.

Several highly filled zones are also observed as indicated by the arrow in Figure 2. In Figure 5a, the filler structure in such a zone is shown at high magnification. Electron microscopy demonstrates that these zones contain polymer, and can thus be swollen. Indeed in Figure 5b, one can see denser regions corresponding to these zones in the swollen sample.

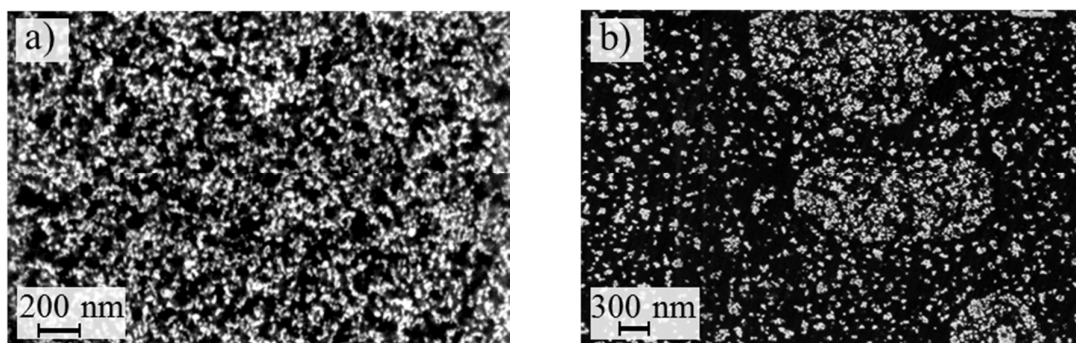


Figure 5: SEM (a) of a silica-SB nanocomposite at high magnification showing the filler network structure inside a highly filled zone ($\Phi_{\text{Si}} = 16.8\%v$, 50%D3), (b) of the same sample highlighting the swelling of the highly filled zones ($\Phi_{\text{Si}} = 2.0\%v$).

To summarize the electron microscopy results, the minority population of highly filled zones can be swollen, whereas the vast majority of the PNCs contain a homogeneous filler network, which is disintegrated into aggregates upon swelling.

In order to go beyond these qualitative results, a more quantitative and statistically significant analysis has been performed. Small-angle scattering is a powerful tool to investigate filler structure in samples at all stages, before and after the swelling procedure. Since swelling generates large inter-particle distances, the SAXS experiments should enable a direct

measurement of the form factor of aggregates in the original material, and thus their average mass and shape. In Figure 6, a newly formulated nanocomposite series is shown for different silica volume fractions and identical matrix composition (50%D3), as studied before²³. In order to avoid the complete dissolution of nanocomposites by swelling with the solvent, the samples have been crosslinked following the procedure given in the experimental section. As can be seen in Figure 6 for the lowest and highest silica content, the effect of crosslinking on the silica microstructure is found to be weak. Scattering in both the high and the low- q regimes superimpose rather well, and the minor difference around the shoulder indicates that the size and shape of aggregates remains mostly unchanged upon crosslinking.

In order to check the similarity in aggregate structure, the previously published results²³ are compared to the present ones for two nanocomposites at low (8.2%v) and high (21.3%v) silica contents in the inset of Figure 6. For both Φ_{Si} , the reduced scattered intensities, $I(q)/\Phi_{Si}$, of the initial unswollen nanocomposites are found to be very close to the previously observed one. In particular, both the high- q and the low- q regimes coincide, which proves that both the local structure – NP and internal organization of filler aggregates – and the large-scale structure – fractal networks – are identical. The new nanocomposites display a slightly higher intensity of the intermediate- q shoulder, around $3 \cdot 10^{-3} \text{ \AA}^{-1}$, evidencing a marginally higher compacity as we will see from the application of the structural model below. It can thus be concluded from the comparisons in Figure 6 that the nanocomposites produced for the present study have the same microstructure as before, and that it is unchanged upon crosslinking.

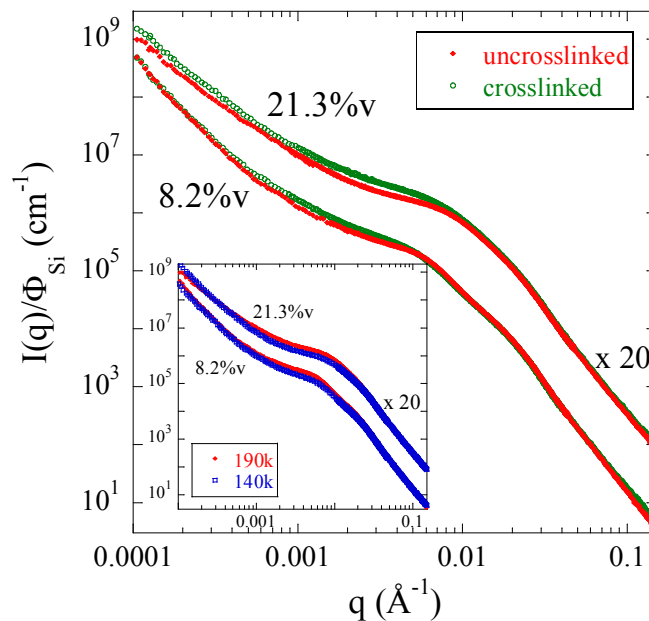


Figure 6: Comparison of filler microstructure as seen by SAXS before (red) and after (green curves) crosslinking for the 8.2%v and 21.3%v-nanocomposites. Curves have been shifted for clarity as indicated. In the inset, new 190k-samples are compared to previously measured 140k-nanocomposites²³.

After crosslinking, nanocomposite samples have been swollen with styrene and polymerized as illustrated in Figure 1. In agreement with the low silica fractions (Table 2), the resulting SAXS intensities are much weaker. However, by normalizing to the experimental Φ_{Si} , the latter can be brought to superposition in the high- q range as shown in Figure 7.

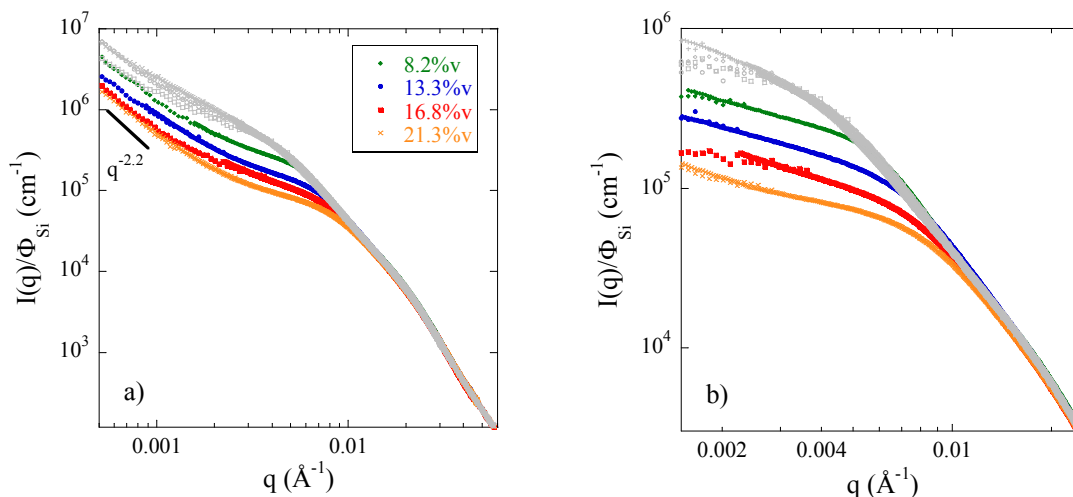


Figure 7: (a) Comparison of microstructure of unswollen (plain, colored symbols) and swollen (empty, grey symbols) nanocomposites for the series in silica volume fraction at 50%D3. SAXS intensities are renormalized to the effective silica volume fraction (8%v to 21%v as indicated in the legend) after subtraction of the corresponding matrix. **(b)** The same data of nanocomposites after subtraction of the fractal network contribution ($q^{-\alpha}$, with $\alpha = 2.2 \pm 0.1$ depending on samples).

There are two families of curves shown in Figure 7. First, the raw data of the unswollen series is shown in Figure 7a (colored symbols): in the intermediate q -range, the normalized intensities decrease with increasing filler fraction, which was successfully modelled in Ref. ²³ by the growing contribution of the repulsive inter-aggregate structure factor. Indeed, our structural model decorrelates in a self-consistent way the evolution of form factor describing aggregate size, and the structure factor, which is due to inter-aggregate interactions. The model shows that the form factor is mostly unchanged in nanocomposites of different volume fraction. In other words, aggregates were merely concentrated but not reorganized internally (besides a slight densification), contrary to what one could expect from the radically different mixing viscosities at various Φ_{Si} . In Figure 7b, the same data of the unswollen nanocomposites is plotted after subtraction of the matrix and the low- q network contribution, in order to apply the model in the intermediate q -range ($q = 3 \cdot 10^{-3} \text{ \AA}^{-1}$). The results of the structural model are summarized in Table 4.

Table 4: Average aggregate radius, average aggregation number, and compacity for a series of nanocomposites at different silica volume fractions (50%D3, no swelling).

Φ_{Si} (%v)	$\langle R_{agg} \rangle$ (nm)	$\langle N_{agg} \rangle$	κ
8.2	39.1	52	34%
13.3	35.4	46	40%
16.8	34.5	44	41%
21.3	32.4	37	42.5%

As compared to our previous study ²³, the average aggregation number of the silica aggregates stays in the same range, about 45, and the average aggregate radius decreases from about 40 nm to 32 nm. The combination of size and mass yields the compacity, which is found to increase slightly from 34 to 43%. As already noted in the comparison in the inset of Figure 6, the new samples are thus structurally very similar to the previous ones.

The second series is shown in the same plots, see Figure 7a and b. After swelling and styrene polymerization, the normalized intensities now overlap rather nicely over almost the entire q -range. This constitutes the main result of the present study: Diluting the sample via the swelling procedure amounts to reducing interactions and shows that aggregates are mostly identical in spite of the different original Φ_{Si} . Ideally, swelling was expected to reduce the inter-aggregate structure factor to one, and to allow measuring the form factor. In Figure 7b, the intensity data of swollen nanocomposites have been plotted after subtraction of the

independently measured matrix contribution, and the low- q power law describing the large-scale network of aggregates. The intensities are seen to level off to a quasi-plateau at intermediate q , which is the origin of the shoulder in the scattered intensity in Figure 7a. It turns out, however, that the very low- q scattering does not overlap perfectly in Figure 7b. This can be understood from the swelling procedure, and the swelling ratio given in Table 2. Indeed, swelling is not equivalent to diluting the sample as one would dilute a colloidal solution, where lower concentrations imply a lower degree of order. Here, the pair correlation function is more probably simply stretched, corresponding to an affine displacement of all centers-of-mass of aggregates, without disturbing the correlation. The swelling ratio of about a factor of 10 leads to an extension by $10^{1/3}$ of the pair correlation function, and thus to a corresponding compression of $S(q)$. Unfortunately, this is not sufficient to obtain a structure factor of one in the q -range of interest: swelling moves the low- q regime of $S(q)$ out of reach, without reaching the high- q regime where $S(q) = 1$. Another consequence is that the aggregate size determination is also hindered by the variations of $S(q)$ in the relevant q -range. We must conclude that even if the qualitative result in Figure 7 is convincing, our model should not be appropriate for extracting compacity and aggregate characteristics from these scattering curves with high precision. For the sake of completeness, we have nonetheless applied our model to the data of swollen samples. From the intensity value, N_{agg} is found to be in the 20 – 30 range, which might even agree with the TEM pictures (for 100%D3) shown in Figure 4. Secondly, the aggregate size determined from the Kratky plots increases slightly (e.g., from 39 to 43 nm and from 32 to 33 nm for $\Phi_{\text{Si}} = 8.2$ and 21.3%v, respectively). This appears to be in line with the SEM/TEM pictures shown in Figures 3b and 4, but one needs to keep in mind that this value is probably too high, and minor changes in R_{agg} affect the compacity strongly because $N_{\text{agg}} = \kappa(R_{\text{agg}}/R_{\text{Si}})^3$. The resulting compacity κ is far too low, about 15%, presumably due to the high value of R_{agg} , whereas the TEM pictures indicate values in the range $\kappa \approx 30 - 40\%$. The latter value also agrees with the model results of unswollen samples reported in Table 4. From the combined analysis of the TEM and SAXS data, it thus appears that aggregates are separated by swelling, sufficiently for the TEM to recognize individual aggregates having characteristics typically found in the unswollen state, but insufficiently to apply the structural model to the swollen state due to remaining interferences of the structure factor. Concerning the value of N_{agg} after swelling, which might suggest that aggregates have been partially destroyed by the swelling procedure, this should be seen with caution as the value is deduced from the model which does not apply perfectly well to this case of

intermediate dilution. Also, N_{agg} is too close to the one of the original, unswollen case, making a clear claim impossible.

To summarize, the measurement of the microstructure of swollen nanocomposites validates the results of our original structural model²³. Indeed, after swelling-induced dilution, the intensities superimpose for almost all q in Figure 7b, indicating that the aggregate form factors are identical, in spite of the different filler volume fractions of the initial formulation.

In previous articles, it has been established that the matrix composition (D3/NF) is the key parameter determining the filler structure due to the end-grafting of chains on the silica NPs^{22, 24}. As outlined in the introduction, the size and mass of aggregates was found to decrease with increasing D3-content. The analogous SAXS-results for the system studied here (190 kg/mol) are shown in Figure 8a, before (colored, plain symbols) and after swelling (grey, empty symbols). Before swelling, the large and the low- q data superimpose, but a D3-dependent intermediate- q dependence is found. The higher the density of grafting D3-functions, the lower the intensity level of this shoulder. In the framework of our structural model²³, this has been translated into a decrease in mass and size of filler aggregates²⁴. This can be understood easily, as these nanocomposites have an identical filler content, and thus roughly identical inter-aggregate interactions described by $S(q)$. Accordingly, the decrease observed in Figure 8a is due to the reduction in aggregate mass.

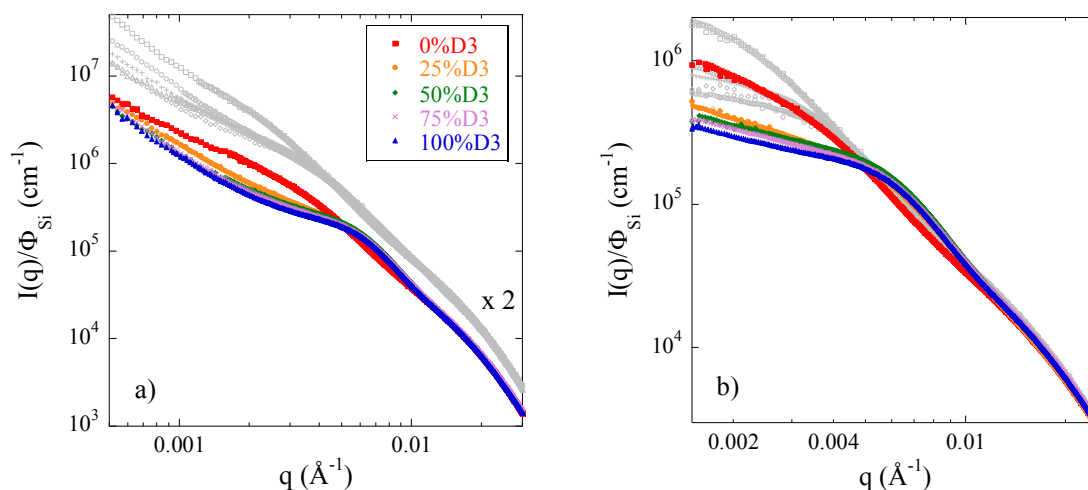


Figure 8: (a) Comparison of microstructure of unswollen (plain, colored symbols) and swollen (empty, grey symbols) nanocomposites for the series in matrix composition (grafting) from 0 to 100%D3, at $\Phi_{\text{Si}} = 8.2\%v$, after subtraction of the corresponding matrix. (b) The same data of nanocomposites after subtraction of the fractal network contribution.

In analogy with Figure 7b, the scattering of the same 8%v-samples before and after swelling is shown in Figure 8b, after subtraction of the matrix and the fractal power law. The observation is the same as in Figure 8a: the differences below ca. 0.005 \AA^{-1} are systematic with the quantity of graftable endfunctions D3, and the decrease in intensity is directly related to that of the aggregate form factor, and thus mass. These measurements on swollen nanocomposites with a variation of grafting density confirm again the results of the structural model applied to the concentrated, unswollen case. Finally, it may be noted that a series analogous to the one shown in Figure 8, but at higher silica volume fraction, confirms our findings (not shown).

4. Conclusion

The complex filler structure of silica nanoparticles in simplified industrial nanocomposites made of styrene-butadiene copolymers with parts of the chains – a fraction termed %D3 – carrying a single endfunction capable of grafting on the silica surface has been investigated by SAXS. Three series of nanocomposites have been formulated with a matrix chain mass of 190 kg.mol^{-1} . The first series at fixed matrix (grafting) composition of 50%D3 was a series in silica volume fraction (8 to 21%v), for which a previously published structural model concluded on the surprising result of mainly identical small aggregates containing some 40 or 50 nanoparticles, independent of Φ_{Si} . The model was based on a self-consistent description of aggregate interactions. In the present article, these results were confirmed by swelling such samples with styrene, thereby reducing aggregate interactions in parts. The dilution has first been illustrated by SEM and TEM pictures. Also, the different steps of our approach – crosslinking, swelling and polymerization – have been monitored carefully, both by electron microscopy and SAXS. The final SAXS analysis of swollen samples shown here confirms in a convincing manner the absence of effect of filler content on aggregate size and shape. Secondly, two series at fixed silica volume fraction (ca 8%v and 17%v) have been investigated, for matrix composition ranging from 0% to 100%D3. In both cases, increasing the grafting fraction leads to smaller aggregates as described by our structural model previously, and again this is confirmed nicely by the SAXS analysis of the swollen samples.

After having established the first structural model of ‘non-model’ polymer nanocomposites with polydisperse silica filler of complex multi-scale structure using a quantitative

combination of SAXS, TEM, and numerical simulations, the challenge was to cross check these results with an independent method. The present article proposes such an approach, based on a physico-chemical manipulation of such nanocomposites (swelling) together with SAXS, and the result gives unambiguous credit to our previous structural analysis. On the other hand, quantitative agreement is not found in terms of aggregation numbers, presumably because our model constructed for concentrated aggregates does not perform well in the diluted domain, in particular at intermediate dilution. Our approach can now be generalized to microstructures of increasing complexity, hopefully contributing to a deeper understanding of mechanical properties of more realistic polymer nanocomposites.

Acknowledgements

We are thankful for a “Chercheur d’Avenir” grant by the Languedoc-Roussillon region (JO) and PhD funding “CIFRE” by Michelin (GPB). Parts of the swelling experiments have been prepared by A. Garnero during her internship supervised by NPP and MC. SAXS experiments have been performed on beamline ID02 at ESRF, with help by T. Narayanan and M. Sztucki. ACG and JO acknowledge support by ANR under Contract No. ANR-14-CE22-0001-01 (NANODYN).

References

- 1 J. E. Mark, B. Erman and F. R. Eirich, *Science and Technology of Rubber*. Academic Press: San Diego, 1994.
- 2 J. Jancar, J. F. Douglas, F. W. Starr, S. K. Kumar, P. Cassagnau, A. J. Lesser, S. S. Sternstein and M. J. Buehler, Current issues in research on structure-property relationships in polymer nanocomposites. *Polymer*, 2010, **51**, 3321-3343.
- 3 N. Jouault, P. Vallat, F. Dalmas, S. Said, J. Jestin and F. Boue, Well-Dispersed Fractal Aggregates as Filler in Polymer-Silica Nanocomposites: Long-Range Effects in Rheology. *Macromolecules*, 2009, **42**, 2031-2040.
- 4 C. Chevigny, J. Jestin, D. Gigmes, R. Schweins, E. Di-Cola, F. Dalmas, D. Bertin and F. Boue, "Wet-to-Dry" Conformational Transition of Polymer Layers Grafted to Nanoparticles in Nanocomposite. *Macromolecules*, 2010, **43**, 4833-4837.

- 5 M. Tatou, A. C. Genix, A. Imaz, J. Forcada, A. Banc, R. Schweins, I. Grillo and J. Oberdisse, Reinforcement and polymer mobility in silica-latex nanocomposites with controlled aggregation. *Macromolecules*, 2011, **44**, 9029-9039.
- 6 A. Banc, A. C. Genix, M. Chirat, C. Dupas, S. Caillol, M. Sztucki and J. Oberdisse, Tuning structure and rheology of silica-latex nanocomposites with the molecular weight of matrix chains: a coupled SAXS-TEM-simulation approach. *Macromolecules*, 2014, **47**, 3219–3230.
- 7 A. Papon, S. Merabia, L. Guy, F. Lequeux, H. Montes, P. Sotta and D. R. Long, Unique Nonlinear Behavior of Nano-Filled Elastomers: From the Onset of Strain Softening to Large Amplitude Shear Deformations. *Macromolecules*, 2012, **45**, 2891-2904.
- 8 S. K. Kumar, N. Jouault, B. Benicewicz and T. Neely, Nanocomposites with Polymer Grafted Nanoparticles. *Macromolecules*, 2013, **46**, 3199-3214.
- 9 N. Jouault, F. Dalmas, F. Boue and J. Jestin, Multiscale characterization of filler dispersion and origins of mechanical reinforcement in model nanocomposites. *Polymer*, 2012, **53**, 761-775.
- 10 J. Oberdisse, Aggregation of colloidal nanoparticles in polymer matrices. *Soft Matter*, 2006, **2**, 29-36.
- 11 G. Capuano, G. Filippone, G. Romeo and D. Acierno, Universal Features of the Melt Elasticity of Interacting Polymer Nanocomposites. *Langmuir*, 2012, **28**, 5458-5463.
- 12 L. Staniewicz, T. Vaudey, C. Degrandcourt, M. Couty, F. Gaboriaud and P. Midgley, Electron tomography provides a direct link between the Payne effect and the inter-particle spacing of rubber composites. *Scientific Reports*, 2014, **4**, 7389.
- 13 J. Oberdisse, P. Hine and W. Pyckhout-Hintzen, Structure of interacting aggregates of silica particles for elastomer reinforcement. *Soft Matter*, 2007, **2**, 476-485.
- 14 D. W. Schaefer, T. Rieker, M. Agamalian, J. S. Lin, D. Fischer, S. Sukumaran, C. Y. Chen, G. Beaucage, C. Herd and J. Ivie, Multilevel structure of reinforcing silica and carbon. *Journal of Applied Crystallography*, 2000, **33**, 587-591.
- 15 S. S. Choi, I. S. Kim, S. G. Lee and C. W. Joo, Filler-polymer interactions of styrene and butadiene units in silica-filled styrene-butadiene rubber compounds. *Journal of Polymer Science Part B-Polymer Physics*, 2004, **42**, 577-584.
- 16 J. Ramier, C. Gauthier, L. Chazeau, L. Stelandre and L. Guy, Payne effect in silica-filled styrene-butadiene rubber: Influence of surface treatment. *Journal of Polymer Science Part B-Polymer Physics*, 2007, **45**, 286-298.

- 17 L. Conzatti, G. Costa, M. Castellano, A. Turturro, F. M. Negroni and J. F. Gerard, Morphology and viscoelastic behaviour of a silica filled styrene/butadiene random copolymer. *Macromolecular Materials and Engineering*, 2008, **293**, 178-187.
- 18 Y. Shinohara, H. Kishimoto, N. Yagi and Y. Amemiya, Microscopic Observation of Aging of Silica Particles in Unvulcanized Rubber. *Macromolecules*, 2010, **43**, 9480-9487.
- 19 K. W. Stockelhuber, A. S. Svistkov, A. G. Pelevin and G. Heinrich, Impact of Filler Surface Modification on Large Scale Mechanics of Styrene Butadiene/Silica Rubber Composites. *Macromolecules*, 2011, **44**, 4366-4381.
- 20 A. Mujtaba, M. Keller, S. Ilisch, H. J. Radusch, T. Thurn-Albrecht, K. Saalwachter and M. Beiner, Mechanical Properties and Cross-Link Density of Styrene-Butadiene Model Composites Containing Fillers with Bimodal Particle Size Distribution. *Macromolecules*, 2012, **45**, 6504-6515.
- 21 G. P. Baeza, A. C. Genix, C. Degrandcourt, J. Gummel, M. Couty and J. Oberdisse, Mechanism of aggregate formation in simplified industrial silica styrene-butadiene nanocomposites: effect of chain mass and grafting on rheology and structure. *Soft Matter*, 2014, **10**, 6686-6695.
- 22 G. P. Baeza, A. C. Genix, C. Degrandcourt, J. Gummel, A. Mujtaba, K. Saalwachter, T. Thurn-Albrecht, M. Couty and J. Oberdisse, Studying twin-samples provides evidence for a unique structure-determining parameter in simplified industrial nanocomposites. *ACS Macro Letters*, 2014, **3**, 448-452.
- 23 G. P. Baeza, A. C. Genix, C. Degrandcourt, L. Petitjean, J. Gummel, M. Couty and J. Oberdisse, Multiscale Filler Structure in Simplified Industrial Nanocomposite Silica/SBR Systems Studied by SAXS and TEM. *Macromolecules*, 2013, **46**, 317-329.
- 24 G. P. Baeza, A. C. Genix, C. Degrandcourt, L. Petitjean, J. Gummel, R. Schweins, M. Couty and J. Oberdisse, Effect of Grafting on Rheology and Structure of a Simplified Industrial Nanocomposite Silica/SBR. *Macromolecules*, 2013, **46**, 6388-6394.
- 25 L. Timochenco, V. G. Grassi, M. Dal Pizzol, J. M. Costa, L. G. Castellares, C. Sayer, R. A. F. Machado and P. H. H. Araujo, Swelling of organoclays in styrene. Effect on flammability in polystyrene nanocomposites. *Express Polymer Letters*, 2010, **4**, 500-508.
- 26 A. Boukerrou, J. Duchet, S. Fellahi, M. Kaci and H. Sautereau, Morphology and mechanical and viscoelastic properties of rubbery epoxy/organoclay montmorillonite nanocomposites. *Journal of Applied Polymer Science*, 2007, **103**, 3547-3552.

- 27 H. Acharya and S. K. Srivastava, Influence of nanodispersed organoclay on rheological and swelling properties of ethylene propylene diene terpolymer. *Macromolecular Research*, 2006, **14**, 132-139.
- 28 S. S. Sarkawi, W. K. Dierkes and J. W. M. Noordermeer, Elucidation of filler-to-filler and filler-to-rubber interactions in silica-reinforced natural rubber by TEM Network Visualization. *European Polymer Journal*, 2014, **54**, 118-127.